Progress in Organic Coatings 163 (2022) 106667

Contents lists available at ScienceDirect

Progress in Organic Coatings

journal homepage: www.elsevier.com/locate/porgcoat

# Interfacial, electrical, and mechanical properties of MWCNT in polyurethane nanocomposite coating *via* 2D electrical resistance mapping for aircraft topcoat

Jong-Hyun Kim [a,b], Dong-Jun Kwon [b], K. Lawrence DeVries [c], Joung-Man Park [a,b,c,*]

[a] Department of Materials Engineering and Convergence Technology, Gyeongsang National University, Jinju, Republic of Korea
[b] Research Institute for Green Energy Convergence Technology, Gyeongsang National University, Jinju, Republic of Korea
[c] Department of Mechanical Engineering, The University of Utah, Salt Lake City, UT 84112, USA

ARTICLE INFO

*Keywords:*
MWCNT/PU nanocomposite coating
Interfacial adhesion
2D electrical resistance mapping
Dispersion
Topcoat

ABSTRACT

Interfacial, electrical, and mechanical properties of polyurethane (PU)-type aircraft topcoat layers for LSP (Lightning Strike Protection) was evaluated by 2-D electrical resistance (ER) mapping with different oxidation times. Multi-wall carbon nanotubes (MWCNT) were treated using hydrogen peroxide to improve dispersion. Mechanical property of MWCNT/PU topcoat was determined *via* thin film tensile test, and oxidation degree was determined using TGA and EDS. Static contact angle measurements were used to evaluate work of adhesion between MWCNT and PU coating layer. Interfacial adhesion between MWCNT and PU coating layer was obtained *via* pull-out test and both results were consistent with different MWCNT oxidation times. Electrical properties of MWCNT/PU topcoats were evaluated by surface ER. Surface ER was the lowest at 5 days oxidation times. Higher tensile strength of MWCNT/PU topcoat could contribute to higher interfacial adhesion. Visualization was used to determine MWCNT dispersion and verified successfully using the color variation of 2D ER mapping.

## 1. Introduction

The lightning strike to an aircraft is not uncommon and it poses a potential threat to flight safety that must be recognized [1,2]. If the aircraft surface is not well-protected, the strike causes severe consequences such as vaporization of metal control cables and/or other critical aircraft parts [3,4]. The use of fiber-reinforced composite materials, to reduce weight, raises the issue of damage due to lightning strikes since fiber-reinforced composite materials have significantly lower electrical conductivity (EC) than metallic materials [4,5]. Primarily two methods have been used to study for the solutions on this problem: improve the EC of carbon fiber reinforced composites (CFRC) used in the aircraft structures [6–9]; and to improve the EC of topcoats and primers that are applied to the aircraft's surface [10–13]. The improvement in EC of CFRC using nanoparticle addition has another problem with increasing weight and increasing processing costs. The method of improvement EC of paint layer has also been studied with the addition of conductive particles. Metallic nanoparticles were used as reinforcement because the materials so produced had excellent electrical conductivity [10,11]. However, this material has problems including as follows. First, corrosion was accelerated in metal-based objects such as bolts and nuts used to connect the CFRC structures. Second, fuel efficiency was reduced as the structural weight is increased. Third, the EC was not maintained for long time because the metallic nanoparticles were attacked by chemical exposure such as acid rain and salt water [12,13]. Because of these problems, some recent researchers have attempted to use carbon-based nanoparticles [12–14].

If the carbon-based nanoparticles are used for the reinforcement to improve LSP properties of paint layers, uniform dispersion of the carbon-based nanoparticles is reported to be important [15,16]. The carbon-based nanoparticles were well aggregated in the polymeric resin due to their high hydrophobicity surface [17,18]. The decrease in mechanical and electrical properties of carbon-based nanoparticle added polymeric resin was studied [19,20]. The dispersion of nanoparticles has been improved by the use of various dispersion methods [21–24] and surface treatments [25–29]. A new manufacturing method was developed to improve MWCNT dispersion in a polymeric coating layer. In the manufacturing processes, the MWCNT could be aggregated due to the filtration in narrow gaps of spray gun nozzle [21–24]. To resolve this problem, the surface treatment of carbon-based nanoparticles has been

* Corresponding author at: Department of Materials Engineering and Convergence Technology, Gyeongsang National University, Jinju, Republic of Korea.
*E-mail address:* jmpark@gnu.ac.kr (J.-M. Park).

https://doi.org/10.1016/j.porgcoat.2021.106667
Received 18 September 2021; Received in revised form 22 November 2021; Accepted 6 December 2021
Available online 15 December 2021

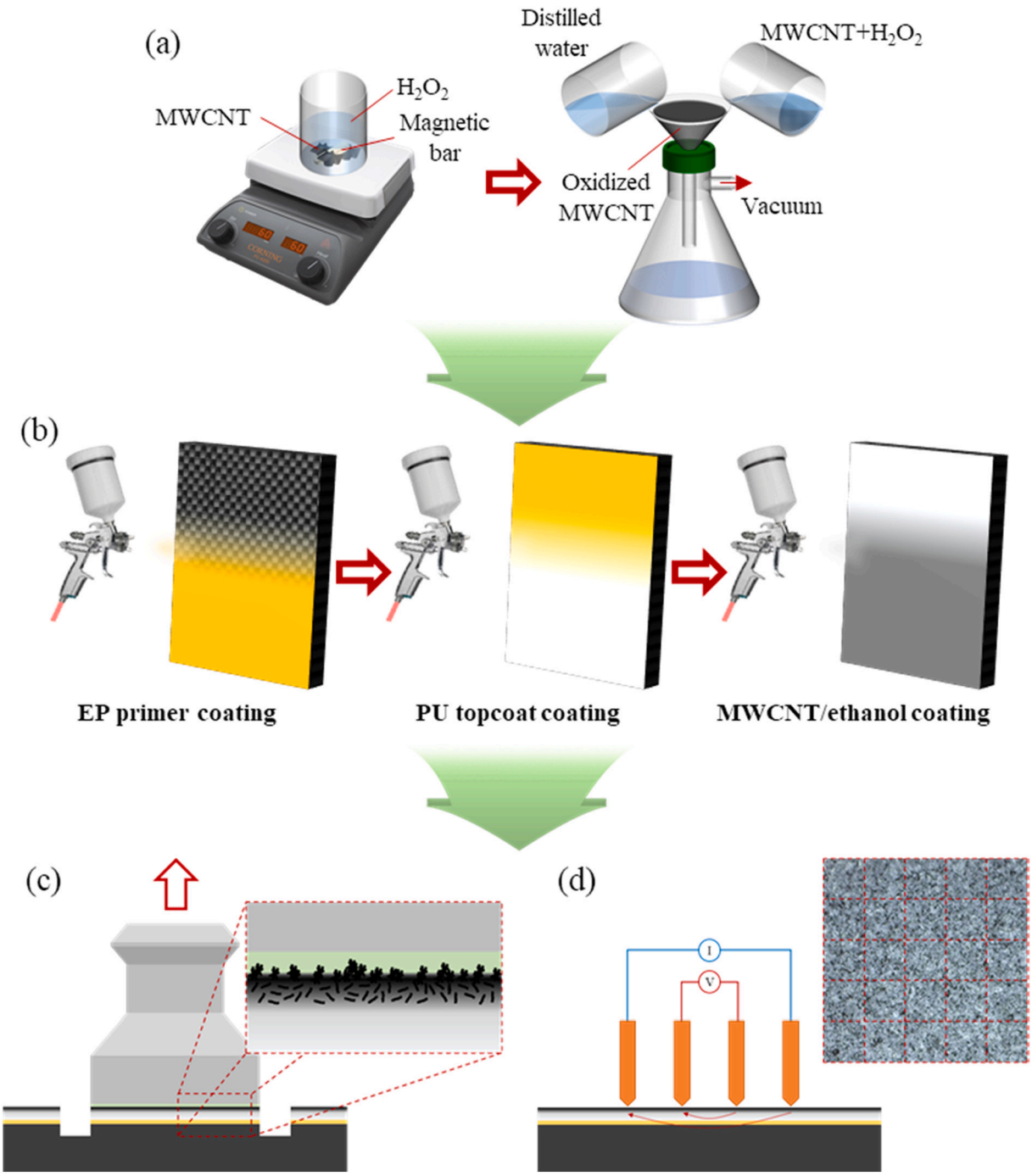


**Fig. 1.** Schematic arrangement of (a) the oxidation of MWCNT using hydroperoxide; (b) the manufacturing process of the MWCNT/PU topcoat; (c) the adhesion pull-off test; and (d) the surface ER measurement of the MWCNT/PU topcoat

tried as a mean of obtaining uniform dispersion using acid, base, and coupling agents. However, MWCNT was damaged during such treatments. This method exhibited other disadvantages such as release of toxic emissions and being difficult to control [25]. In other research, the MWCNT has been modified using a coupling agent. In this method, the MWCNT was pre-modified using an acid to create reaction sites for the coupling agent [26,27]. Currently, a simple and eco-friendly surface treatment method has been suggested for the modification of CNT, where hydrogen peroxide was the only required chemical and no toxic emissions were released [28,29].

In this paper, ER, adhesion and dispersion properties of MWCNT were evaluated for different MWCNT oxidation times. MWCNTs used for the reinforcement and polyurethane (PU) topcoat for aircraft were used as matrices. MWCNT was modified and dispersed uniformly in the PU topcoat *via* the ultrasonication and the oxidation of MWCNT was studied using thermos-gravimetric analysis (TGA) and energy dispersive spectrometer (EDS). The mechanical property of MWCNT/PU topcoat was evaluated using thin film tensile test. The surface energies and work of adhesion, $W_a$ for neat and MWCNT/PU topcoats were evaluated using static contact angle measurement. Adhesion properties were evaluated using adhesion pull-off test with different MWCNT oxidation times. The dispersion of the MWCNT and electrical properties were visualized using 2D ER mapping. The MWCNT oxidation time was optimized to decrease the ER of MWCNT/PU topcoat. Finally, the optimized MWCNT

condition was determined to improve adhesion and electrical properties with different MWCNT oxidation time for LSP of aircraft. MWCNT could alternate the metallic materials if the MWCNT dispersion was improved further.

## 2. Experimental

### 2.1. Materials and specimen preparation

MWCNT (20 nm in diameter, 10 μm in length, Carbon Nano-Material Technology Co. Ltd., Korea) was used as a reinforcement to improve EC, for the matrix of PU type topcoat for aircraft (MIL-PRF-85285D, Hentzen Coatings, USA). As illustrated in Fig. 1(a), the oxidation of MWCNT involved the use of hydrogen peroxide (Duksan Pure Chemicals Co., Korea) at a ratio 1.5 g MWCNT: 30 mL hydrogen peroxide. The MWCNT/hydrogen peroxide mixture was stirred, at 60RPM, on a hotplate (PC 620D, Corning Inc., USA) at 60 °C for 3 days with 5 mL the hydrogen peroxide added each day. The MWCNT was then filtered and rinsed using a distilled water before drying at 40 °C for 24 h in the drying oven (OF-22GW, Jeio Tech Co. Inc., Korea) in a vacuum with a desiccator [26,27]. MWCNT was dispersed in ethanol using an ultrasonicator (VC-505, Sonics & Materials Inc. USA) for 90 min. As illustrated in Fig. 1(b), MWCNT/ethanol solution was sprayed on a 50 × 50 mm area of PU topcoat coated CFRP, which had been pre-cured at 70 °C for 30 min in a drying oven. The MWCNT/PU topcoat was then fully cured in a drying oven at 70 °C for 1 h. The coating layer thickness of EP primer, PU topcoat, and MWCNT coating were measured using the thickness gauge (No.7301, Mitutoyo, Japan), and exhibited 20 μm, 60 μm, and 0.1 μm, respectively.

### 2.2. Methodologies

#### 2.2.1. Mechanical and thermal properties of MWCNT/PU topcoat with different oxidation times

Thermal property of MWCNT was evaluated using TGA (Q5000 IR, TA Instruments Inc., France) to compare oxidation degree of MWCNT. The chemical modification of MWCNT was evaluated using EDS of FE-SEM (JSM-7610F, JEOL Ltd., Japan) with different oxidation time. The mechanical property of MWCNT/PU topcoat was evaluated using thin film tensile test based on ASTM D882 with different oxidation times. The MWCNT/PU topcoat film was manufactured on the release film using the process in which was described in materials and specimen preparation section. Five times tensile test was performed for each case using UTM (LR 10 K, Lloyd Instruments Ltd., U.K.) to get statistically meaningful date, and the strain rate was set as 20 mm/min.

#### 2.2.2. Interfacial adhesion prediction of MWCNT/PU topcoat with different oxidation times

The surface energy and work of adhesion of MWCNT/PU topcoat were calculated to investigate the adhesive property difference between MWCNT coated and neat PU topcoat. Static contact angles were measured using 4 solvents, *i.e.* distilled water, ethylene glycol, formamide, and diiodomethane. MWCNT coated and neat PU topcoats were placed on a horizontal stage and a 1 mm diameter-droplet was placed on each of the specimens using a syringe. The static contact angle of solvent droplets was measured using a reflecting microscope (AM4113ZT, Anmo Electronics Corporation, Taiwan). The total surface energy, $\gamma^T$ was the sum of the Lifshitz-van der Waals component, $\gamma^{LW}$ and the acid-base component, $\gamma^{AB}$. Using these components and following the modified young-Dupre equation [30] of the work of adhesion, $W_a$ can be calculated as:

$$W_a = \gamma_L(1+cos\theta) = 2\left(\gamma_L^{LW}\gamma_S^{LW}\right)^{\frac{1}{2}} + 2\left[\left(\gamma_S^-\gamma_L^+\right)^{\frac{1}{2}} + \left(\gamma_S^+\gamma_L^-\right)^{\frac{1}{2}}\right] \quad (1)$$

A commonly-used approach in considering solid surface energies was to express them as a sum of dispersive and polar components which can influence the work of adhesion, $W_a$ between the surface of the reinforcement material and the matrix. To determine the polar and dispersive surface free energies, the Owens-Wendt equation [31] was used as:

$$W_a = \gamma_L(1+cos\theta) = 2\left(\gamma_S^d\gamma_L^d\right)^{\frac{1}{2}} + 2\left(\gamma_S^p\gamma_L^p\right)^{\frac{1}{2}} \quad (2)$$

where $\gamma_L$, $\gamma_L{}^d$, and $\gamma_L{}^p$ are known for the testing liquids and $\gamma_S{}^p$ and $\gamma_S{}^d$ can be calculated from the measured contact angles. Based on the surface energy of the material the work of adhesion between the MWCNT coated and neat PU topcoat was obtained to predict interfacial adhesion. The surface morphology of the MWCNT/PU topcoat was determined using FE-SEM (JSM-7610F, JEOL Ltd., Japan) for different oxidation times.

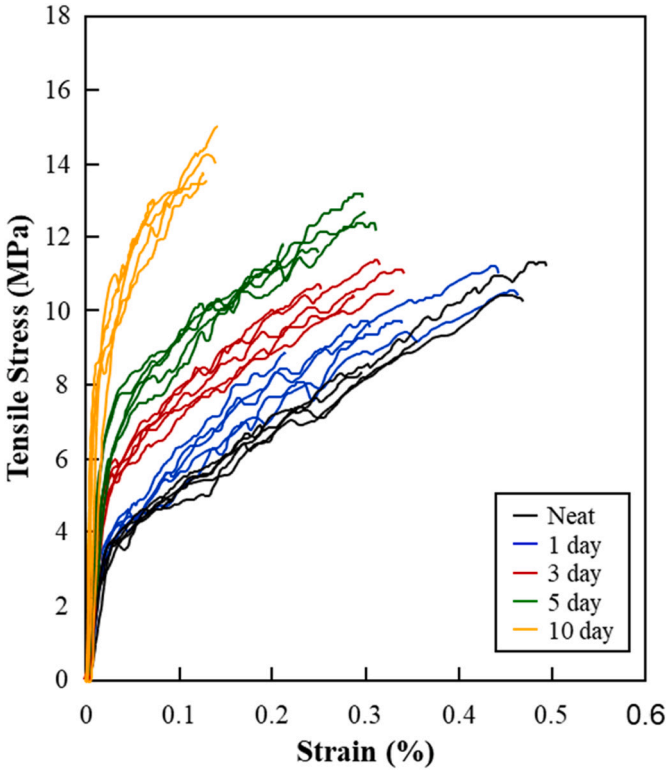


**Fig. 2.** Mechanical property of materials with different oxidation times

#### 2.2.3. Surface roughness and adhesion pull-off test for MWCNT/PU topcoats with different oxidation times

As illustrated in Fig. 1(c), the adhesion was performed based on ASTM D4541 using an adhesion pull-off tester (Elcometer 510, Elcometer Co., USA). The dolly diameter was 20 mm and the pulling rate increased gradually to 0.1 MPa/s. Five tests were performed for each specimen type, to get statistically meaningful data. The metal dolly was attached using the epoxy adhesive (KFR-730FL and KFH-740FL, Kukdo Chemical Ltd., Korea). The specimens were cut near the surface of CFRP so that the attached area would be isolated from the grip section of the specimen.

The surface roughness was determined using a surface roughness tester (SJ-210S, Mitutoyo Co., Japan). It was scanned, over a 20 mm length, at 25 sections with the scan rate set at 0.25 mm/s. The average of the measured surface roughness, $R_a$, was used to compare the surface roughness of MWCNT/PU topcoats with different oxidation times.

#### 2.2.4. Visualization of surface ER for different MWCNT/PU topcoats

In Fig. 1(d), surface ER measurements using the surface ER tester (FPP-RS8, Dasol ENG Co, Korea), based on ASTM D991. The surface ER was measure at twenty-five 10 × 10 mm sections for each specimen type. The surface ER data was obtained using Eq. (3) and it could be

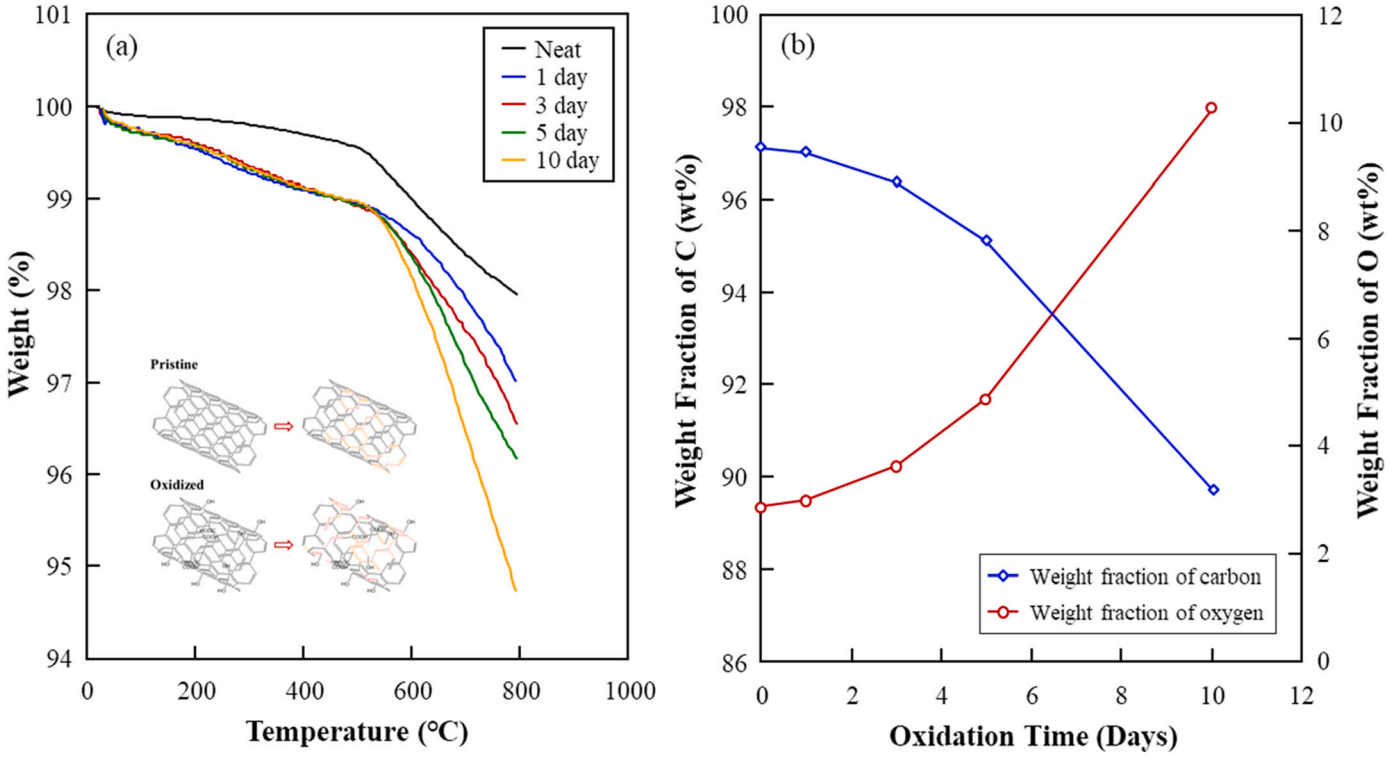


**Fig. 3.** Oxidation degree analysis of MWCNT using: (a) TGA; and (b) EDS with different oxidation times

visualized using a surface chart found in a commercial Excel program.

$$\text{Surface ER variation ratio } (\%) = \frac{(R - R_{average})}{R_{average}} \times 100 \quad (3)$$

where $R$ was the ER at the points of measurement and $R_{average}$ was the average of the ER at all 25 points. The ER and weight variation data were visualized using a surface chart. This chart showed a 2D surface that connected a set of data points for a dispersion condition for the MWCNT with different oxidation times [32].

## 3. Results and discussion

### 3.1. Mechanical and thermal properties of MWCNT/PU topcoat with different oxidation times

In Fig. 2(a), the tensile strength of the MWCNT/PU topcoat exhibits for different oxidation times. The tensile strength increased whereas the strain decreased with increasing the MWCNT oxidation time at yield and fracture points, respectively. As MWCNT oxidation time increased, it could be considered that the surface of MWCNT was modified to be more hydrophilic, and the interfacial property between MWCNT and PU topcoat was improved. In the case of 3 days of the oxidation, the largest standard deviations (SD) of tensile properties exhibited. It could be due to the MWCNT aggregation based on van der Walls force and hydrophobic surface of MWCNTs. The MWCNT was aggregated during the post-curing process, and the aggregation might cause to the crack propagation more easily.

In Fig. 3(a), the TGA plots of oxidized MWCNT exhibited *versus* temperature with different oxidation times. For pristine MWCNT, the pyrolysis began to change rapidly at approximately 500 °C and the weight of MWCNT decreased to 98% as the temperature increased to 800 °C. With increased MWCNT oxidation times, the rate of weight decrease also increased. For MWCNT oxidized for 10 days during the TGA experiments, *e.g.*, the weight of the MWCNT decreased to approximately 95% of its original value as the temperature increased to 800 °C.

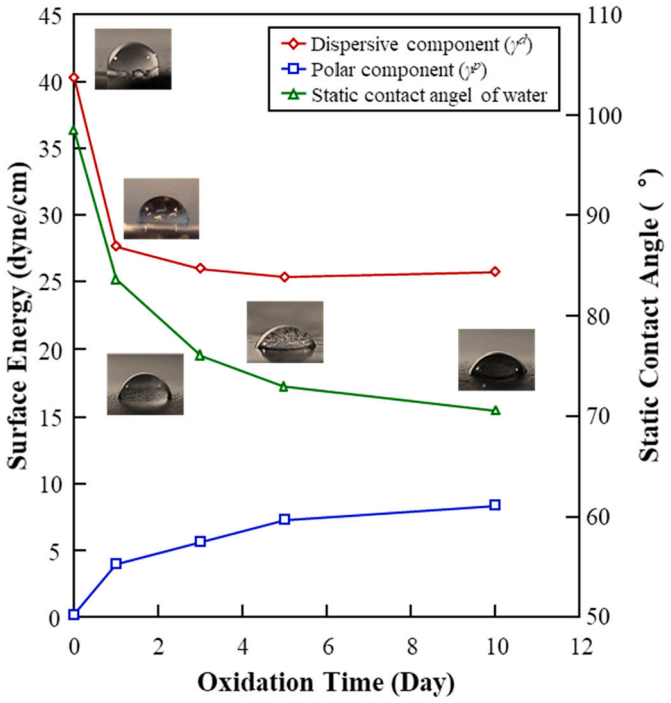


**Fig. 4.** Surface energy and work of adhesion between the EP primer and the MWCNT/PU topcoat with different oxidation times

It was found that the MWCNT oxidized for 10 days was degraded rather rapidly by more than 3.5% of its original weight between about 500 °C and 600 °C. This was thought probably to be due to the breaking of the main chains during the oxidation process.

In Fig. 3(b), atomic element percentages of the neat and oxidized MWCNTs was characterized by EDS analysis to quantify the oxygen

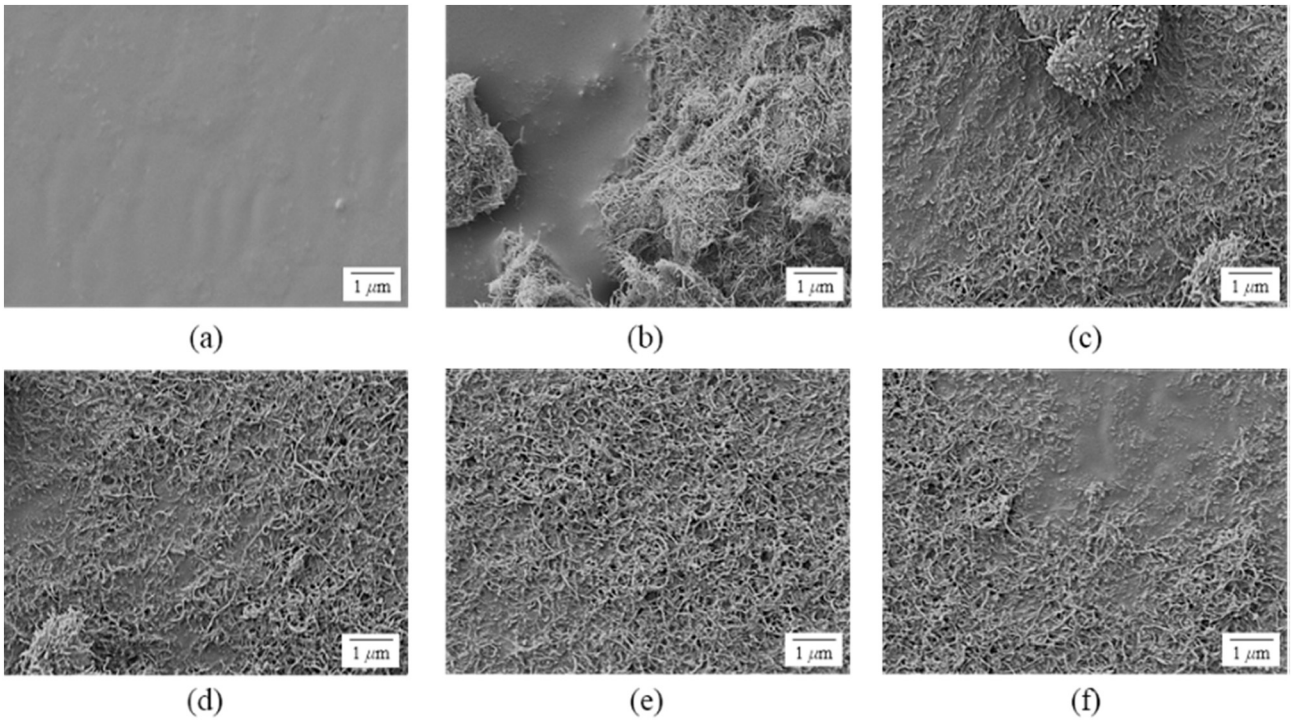


**Fig. 5.** FE-SEM photos of MWCNT/PU topcoat surfaces with different oxidation times: (a) Neat PU; (b) pristine MWCNT coated; (c) 1 day; (d) 3 days; (e) 5 days; and (f) 10 days oxidized MWCNT coated

content of the modified MWCNTs. As the oxidation time of MWCNT increased, the weight fractions of carbon decreased gradually from 99% to 89.3%, whereas the oxygen content increased from 2.4% to 10.2% by the surface modification to introduce hydroxyl and carboxyl groups.

### *3.2. Surface energies and work of adhesion of oxidized MWCNT/PU topcoat with different oxidation times*

The surface energies and work of adhesion, $W_a$ of MWCNT coated

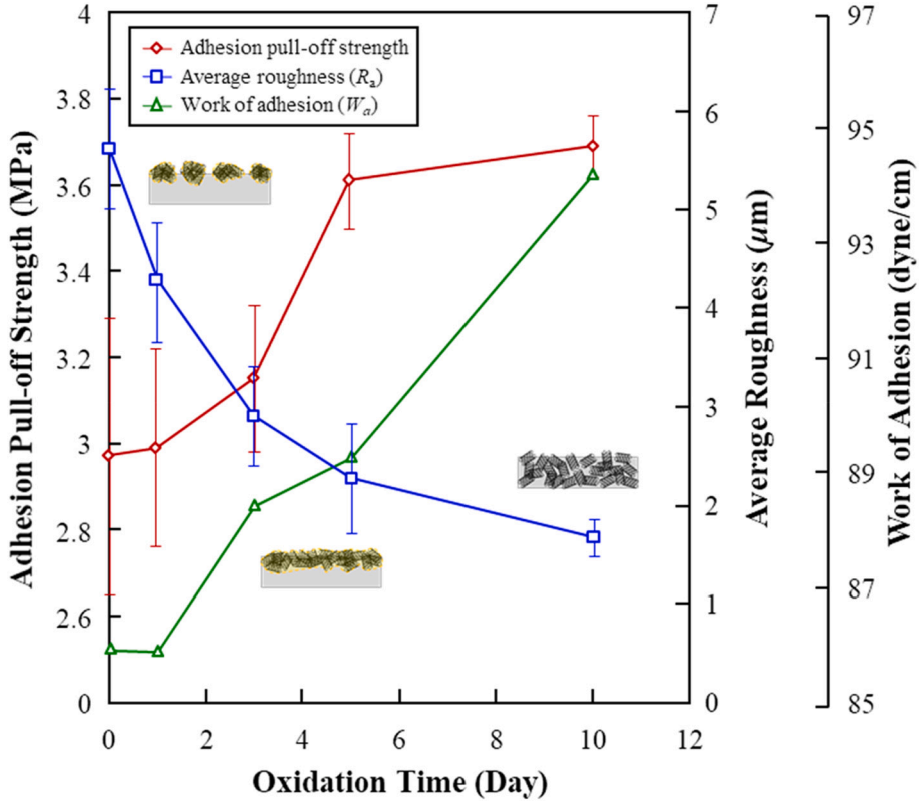


**Fig. 6.** Adhesion and surface roughness of MWCNT/PU topcoat with different oxidation times

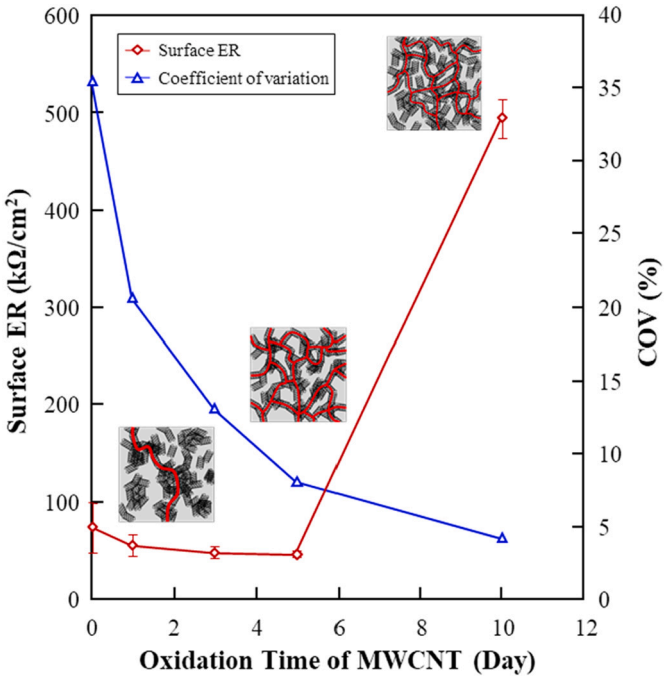


**Fig. 7.** Surface ER of MWCNT/PU topcoat with different oxidation time

and neat PU topcoat were evaluated for the different oxidation times. The dispersive and polar components of the surface energies were evaluated and compared to determine the change in surface energy during the oxidation process. The neat PU topcoat exhibited the highest polar and lowest dispersive components of the surface energy. In Fig. 4, the surface of PU topcoat was seen to be more hydrophilic than the MWCNT coated material, and initially the MWCNT/PU topcoat exhibited the highest disperse and the lowest polar components. It could be expected that the initial MWCNT and PU topcoat exhibited the poorest adhesion. In the oxidized MWCNT, however, the polar component of MWCNT/PU topcoat increased while the disperse component decreased with increased MWCNT oxidation time. It was also observed that adhesion increased as the MWCNT oxidation time increased. During oxidation of MWCNT, the hydrophobic carbon double bonds of the main chain were broken and modified to a hydrophilic surface with hydroxyl and carboxyl groups [33–35]. The water contact angle on the MWCNT/PU topcoat surface decreased from 98 to 70° as the MWCNT oxidation time increased which might be attributed to enhanced adhesion between MWCNT and the PU topcoat.

### 3.3. *Surface roughness and adhesion properties of MWCNT/PU topcoat with different MWCNT oxidation times*

Fig. 5 shows FE-SEM photo of MWCNT/PU topcoat surfaces illustrating the dramatic changes in morphology associated with the different MWCNT oxidation times. Fig. 5(a) shows the untreated neat PU surface whereas Fig. 5(b) shows the PU surface to which the pristine MWCNT coating has been applied. However, the MWCNT was aggregated on the PU surface and the MWCNT was not dispersed uniformly to the PU topcoat. Fig. 5(c) to (f) shows the "coated surface" after 1, 3, 5 and 10 day MWCNT oxidation times. It was observed in the 1 and 3 days FE-SEM photos that the MWCNT aggregation was gradually reduced, and at 5 days the oxidized MWCNT was relatively well dispersed on the PU topcoat. At 10 days oxidized MWCNT case, however, the MWCNT was partially impregnated into the PU topcoat. It was concluded that MWCNT oxidation for 5 days was an optimal treatment.

Fig. 6 shows the surface roughness and adhesive properties for the different oxidation times. Surface roughness of the MWCNT/PU topcoat caused the MWCNT aggregation on the topcoat. The average surface roughness decreased from 5.6 μm to 2.2 μm as the oxidation time of the MWCNT increased from 0 to 5 days. When the oxidation time of the MWCNT increased to10 days, the surface roughness of MWCNT/PU topcoat decreased at a reduced rate to 1.7 μm. It appears therefore that

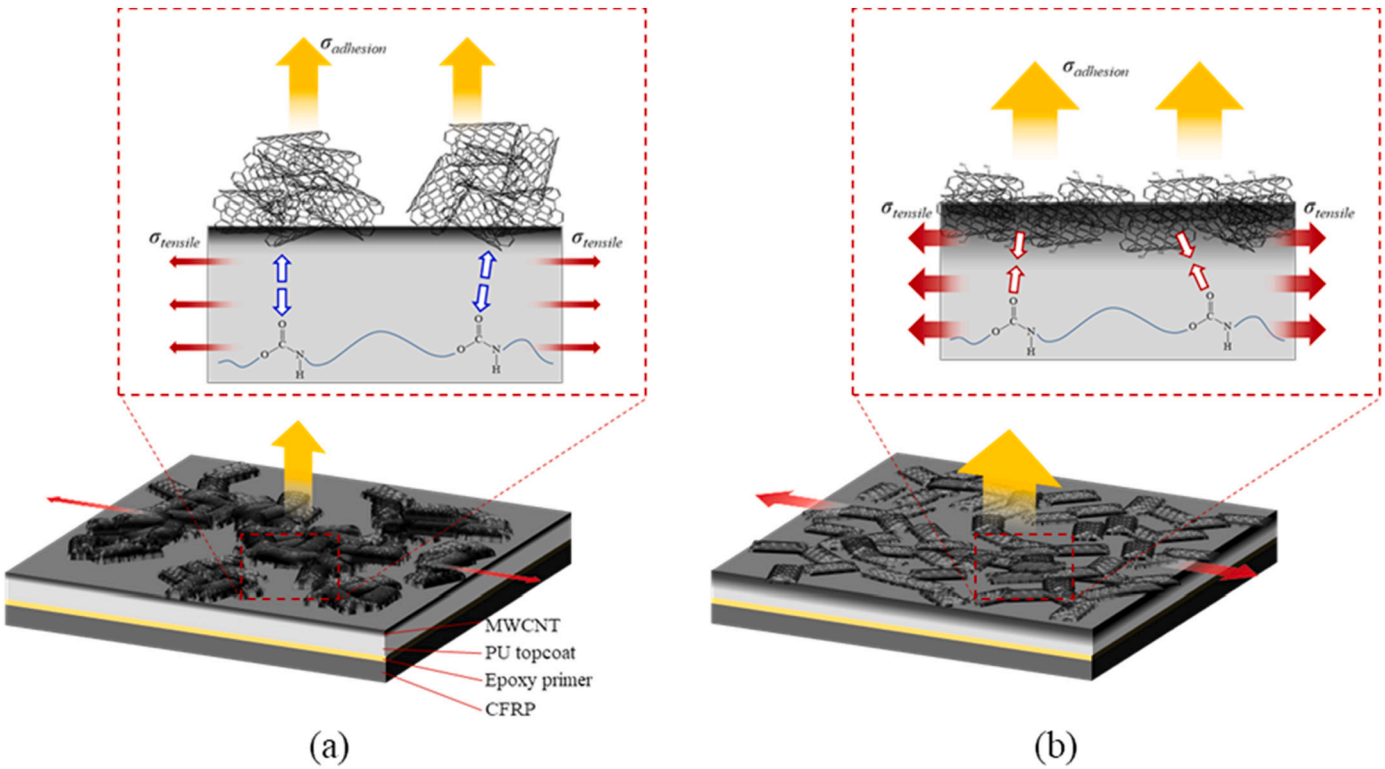


**Fig. 8.** Schematic arrangement of MWCNT/PU topcoat: (a) neat; and (b) oxidized by optimized condition

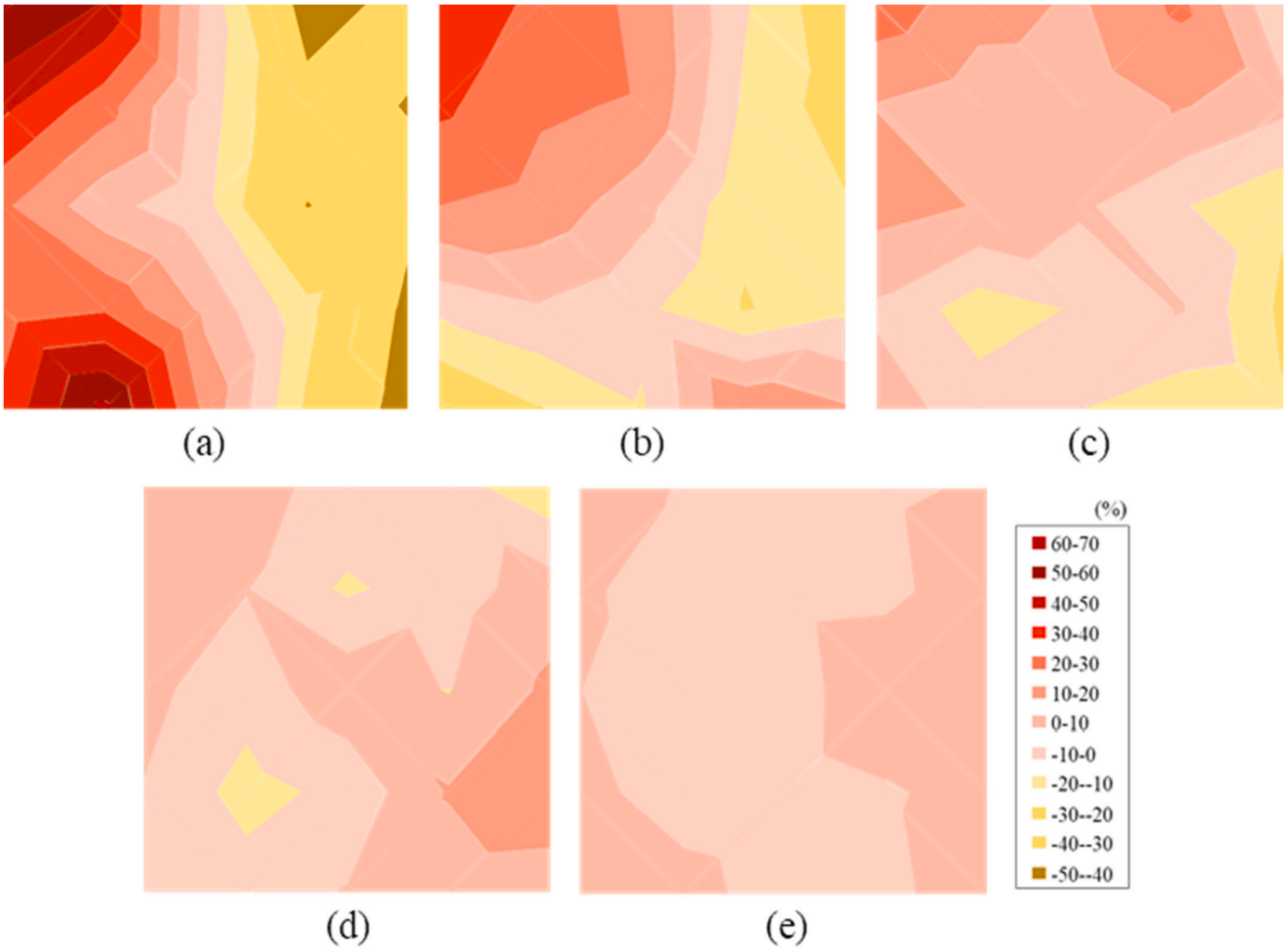


**Fig. 9.** ER mapping of MWCNT/PU topcoat surface with different oxidation time: (a) o; (b) 1 day; (c) 3 days; (d) 5 days; and (e) 10 days

oxidation of MWCNT results in decreased surface roughness of the topcoat. The decrease in surface roughness could likely be attributed to the MWCNT becoming better dispersed and more deeply impregnated in the PU topcoat with the increase in MWCNT oxidation time. Fig. 4 shows that the dispersive component decreased whereas the polar component increased as the MWCNT oxidation time increased. In Fig. 6, it was seen that the work of adhesion increased from 86 to 94 dyne/cm with increasing oxidation times, accompanied by an increase in adhesion pull-out strength. Inversion to the surface roughness this pullout strength rapidly increased from roughly 3.0 MPa to just over 3.6 MPa as the oxidation times increased from 0 to 5 days followed by a very gradual increase to just under 3.7 MPa at 10 days oxidation time.

### 3.4. ER of MWCNT/PU topcoat with different MWCNT oxidation time

Fig. 7 shows the average surface ER and coefficient of variation (COV) for different MWCNT oxidation times. The surface ER of the MWCNT/PU topcoat decreased from roughly 80 kΩ/cm$^2$ to 50 kΩ/cm$^2$ as the MWCNT oxidation time increased from 0 to 5 days, followed by a rapid increase in ER from 530 kΩ/cm$^2$ to 60 kΩ/cm$^2$ for 10 days oxidation time. The surface ER change was related to the dispersion of the MWCNT and the inherent ER of the MWCNT. As the oxidiation time of MWCNT proceeded the hydrophilicity of MWCNT surface increased gradually by introducing hydrophilic groups. The MWCNT dispersion was improved by the oxidation process, and the ER of the MWCNT/PU topcoat decreased gradually due to the improved dispersion of the MWCNT. For 10 days oxidized MWCNT, however, the surface ER increased dynamically to 500 kΩ/cm$^2$. The COV of surface ER decreased as the oxidation time increased. The carbon-carbon double bond of MWCNT was extensively damaged, and the conjugation of MWCNT decreased significantly during the 10 day oxidiation period. The surface ER increased steeply, while the dispersion of MWCNT which was oxidized for 10 days was the better than for the other cases. The MWCNT dispersion could be determined using FE-SEM photos of MWCNT coated PU topcoat in Fig. 6.

As shown in Fig. 8(a), in the case of pristine MWCNT/PU topcoat, the pristine MWCNT was not impregnated to PU topcoat and aggregated to be ‘an island-type’ on PU topcoat. Since poor adhesion occurred, the surface ER of MWCNT/PU topcoat increased due to the decrease in contact points among MWCNTs. In Fig. 8(b), however, the oxidized MWCNT could be impregnated to PU topcoat because of the existing hydrophilic functional groups, such as hydroxy, carboxyl, carbonyl. It resulted in the increased ER of MWCNT possibly due to the fracture of MWCNT main chain during the oxidation process. However, ER of MWCNT/PU topcoat decreased because of the improved dispersion of MWCNTs. The higher tensile strength of MWCNT/PU topcoat could contribute to the higher interfacial adhesion.

In Fig. 9, the dispersion of MWCNT on PU topcoat was visualized using 2D surface ER mapping for different MWCNT oxidiation times. The color variation of the surface ER of MWCNT/PU topcoats decreased from 12 to 2 colors as the MWCNT oxidization time increased. In the case of MWCNT oxidization for 5 days, the hydrophilic group increased near the

surface of MWCNT such as hydroxyl and carboxyl groups. As the oxidizing time increased, however, the surface ER decreased because of improvement of MWCNT dispersion while the ER of MWCNT decreased by breaking the main chains. In the case of MWCNT oxidization for more than 5 days, the main chain of MWCNT might be extensively broken and the ER of MWCNT decreased while the dispersion of MWCNT was improved.

## 4. Conclusions

In this paper, MWCNT was used as a substitute for metallic nanoparticles despite MWCNT having problems with dispersion. The MWCNT was oxidized using hydroperoxide to solve the dispersion problem. The mechanical properties of MWCNT/PU topcoat were evaluated using thin film tensile test. The tensile strength increased as the MWCNT oxidation time increased. The oxidation degree was evaluated using TGA and EDS. The decrease in weight of MWCNT was gradually accelerated as the oxidation time increased and the breaking of MWCNT main chains could occur. The oxygen contents increased and it caused by the oxidation of MWCNT. The surface energies and work of adhesion between MWCNT coated and neat PU topcoat were determined to compare adhesive properties for different MWCNT oxidation times. The polar component and work of adhesion increased with increased oxidation times while the dispersive component decreased. The introduced hydroxyl groups in oxidized MWCNT would forecast an increase in adhesive properties. The adhesion of the MWCNT/PU topcoat was improved by approximately 120% and the adhesion stability increased as the MWCNT oxidation time increased. The surface ER of MWCNT/PU topcoat decreased as the MWCNT oxidation time increased to 5 days. For the 10 days treatment, the surface ER increased steeply, due to main chain breakage during the oxidation process while the MWCNT dispersion improved. The MWCNT dispersion was observed using 2D surface ER mapping technique. The higher tensile strength of MWCNT/PU topcoat could contribute to the higher interfacial adhesion. The MWCNT dispersion in PU topcoat was evaluated using ER mapping, and the range of ER decreased as the MWCNT oxidation time increased. From these results, it was concluded that an oxidation time of 5 days was optimal for LSP aircraft applications and that the dispersion of nanoparticles can be visualized using ER 2D mapping.

## CRediT authorship contribution statement

Jong-Hyun Kim: Writing - Original Draft, Data Curation, Visualization Formal analysis.

Dong-Jun Kwon: Formal analysis, Writing - Review & Editing.

K. Lawrence DeVries: Formal analysis, Writing - Review & Editing.

Joung-Man Park: Formal analysis, Visualization, Writing - Review & Editing, Visualization, Supervision.

## Declaration of competing interest

The authors declare that they have no known competing financial interests or personal relationships that could have appeared to influence the work reported in this paper.

## Acknowledgements

This research was supported by Basic Science Research Program through the National Research Foundation of Korea (NRF) funded by the Ministry of Education, Korea (No. 2016R1D1A1B01012620), 2021–2022.

## References

[1] A. Larsson, The interaction between a lightning flash and an aircraft in flight, C. R. Phys. 3 (2002) 1423–1444, https://doi.org/10.1016/S1631-0705(02)01410-X.

[2] B.D. Fisher, R.J. Taeuber, J.T. Ralph, K.E. Crouch, Implications of a recent lightning strike to a NASA jet trainer, Proc. AIAA 26 (1988) 1–10, https://doi.org/10.2514/6.1988-394.

[3] C.C.R. Jones, D. Rowse, G.A.M. Odam, Probabilities of catastrophe in lightning hazard assessments, Proc. ICOLSE (2001), https://doi.org/10.4271/2001-01-2877.

[4] G. Martin, T. Daniel, Lightning strike protection of composites, Prog. Aerosp. Sci. 64 (2014) 1–16, https://doi.org/10.1016/j.paerosci.2013.07.002.

[5] P. Feraboli, M. Miller, Damage resistance and tolerance of carbon/epoxy composite coupons subjected to simulated lightning strike, Compos. Part A Appl. Sci. Manuf. 40 (2009) 954–967, https://doi.org/10.1016/j.compositesa.2009.04.025.

[6] N. Causse, S. Benchimol, L. Martimeau, D. Carponcin, L. Antoine, M. Fogel, D. Jany, D. Eric, C. Lacabanne, Polymerization study and rheological behavior of a RTM6 epoxy resin system during preprocessing step, J. Therm. Anal. Calorim. 119 (2015) 329–336, https://doi.org/10.1007/s10973-014-4147-y/.

[7] S.C. Schulz, G. Faiella, S.T. Buschhorn, L.A.S.A. Prado, M. Giordano, K. Schulte, W. Bauhofer, Combined electrical and rheological properties of shear induced multiwall carbon nanotube agglomerates in epoxy suspensions, Eur. Polym. J. 47 (2011) 2069–2077, https://doi.org/10.1016/j.eurpolymj.2011.07.022.

[8] G. Olowojoba, S. Sathyanarayana, B. Caglar, B. Kiss-Pataki, M. Irma, C. Hübner, P. Elsner, Influence of process parameters on the morphology, rheological and dielectric properties of three-roll-milled multiwalled carbon nanotube/epoxy suspensions, Polymer 54 (2013) 188–198, https://doi.org/10.1016/j.polymer.2012.11.054.

[9] J. Rehbin, P. Wierach, T. Gries, M. Wiedemann, Improved electrical conductivity of NCF-reinforced CFRP for higher damage resistance to lightning strike, Compos. Part A Appl. Sci. Manuf. 100 (2017) 352–360, https://doi.org/10.1016/j.compositesa.2017.05.014.

[10] P.S.M. Rajesh, F. Sirois, D. Therriault, Damage response of composites coated with conducting materials subjected to emulated lightning strikes, Mater. Des. 139 (2018) 45–55, https://doi.org/10.1016/j.matdes.2017.10.017.

[11] Y. Li, T. Xue, R. Li, X. Huang, L. Zeng, Influence of a fiberglass layer on the lightning strike damage response of CFRP laminates in the dry and hygrothermal environments, Compos. Struct. 187 (2018) 179–189, https://doi.org/10.1016/j.compstruct.2017.12.057.

[12] B. Wang, Y. Duan, Z. Xin, X. Yao, D. Abliz, G. Ziegmann, Fabrication of an enriched graphene surface protection of carbon fiber/epoxy composites for lightning strike via a percolating-assisted resin film infusion method, Compos. Sci. Technol. 158 (2018) 51–60, https://doi.org/10.1016/j.compscitech.2018.01.047.

[13] D.K. Chakravarthi, V.N. Khabashesku, R. Vaidyanathan, J. Blaine, S. Yarlagadda, D. Roseman, Q. Zeng, E.V. Barrera, Carbon fiber-bismaleimide composites filled with nickel-coated single-walled carbon nanotubes for lightning-strike protection, Adv. Funct. Mater. 21 (2011) 2527–2533, https://doi.org/10.1002/adfm.201002442.

[14] W. Yao, K.J. Bae, M.Y. Jung, Y.R. Cho, Transparent, conductive, and superhydrophobic nanocomposite coatings on polymer substrate, J. Colloid Interface Sci. 506 (2017) 429–436, https://doi.org/10.1016/j.jcis.2017.07.071.

[15] C. Pramanik, J.R. Gissinger, S. Kumar, H. Heinz, Carbon nanotube dispersion in solvents and polymer solutions: mechanisms, assembly, and preferences, ACS Nano 11 (2017) 12805–12816, https://doi.org/10.1021/acsnano.7b07684.

[16] C. Feng, S. Kitipornchai, J. Yang, Nonlinear bending of polymer nanocomposite beams reinforced with non-uniformly distributed graphene platelets (GPLs), Compos. B Eng. 110 (2017) 132–140, https://doi.org/10.1016/j.compositesb.2016.11.024.

[17] Y. Liu, Y. Zhang, Z. Wang, W. Lai, X. Zhang, X. Wang, X. Liu, Investigation of the dispersion behavior of fluorinated MWCNTs in various solvents, Phys. Chem. Chem. Phys. 19 (2017) 21565–21574, https://doi.org/10.1039/C7CP04536K.

[18] W. Yuan, Q. Hu, J. Zhang, F. Huang, J. Liu, Hydrophobic modification of graphene oxide and its effect on the corrosion resistance of silicone-modified epoxy resin, Metals 11 (2020) 89–106, https://doi.org/10.3390/met11010089.

[19] Z.J. Wang, D.J. Kwon, G.Y. Gu, W.I. Lee, J.K. Park, K.L. DeVries, J.M. Park, Evaluation of interfacial properties of atmospheric pressure plasma-treated CNT-phenolic composites by dual matrix fragmentation and acoustic emission tests, Compos. Compos. Part A Appl. Sci. Manuf. 52 (2013) 151–158, https://doi.org/10.1016/j.compositesa.2012.07.008.

[20] S. Han, Q. Meng, S. Araby, T. Liu, M. Demiral, Mechanical and electrical properties of graphene and carbon nanotube reinforced epoxy adhesives: experimental and numerical analysis, Compos. Part A Appl. Sci. Manuf. 120 (2019) 116–126, https://doi.org/10.1016/j.compositesa.2019.02.027.

[21] A.H. Baferani, A.A. Katbab, A.R. Ohadi, The role of sonication time upon acoustic wave absorption efficiency, microstructure, and viscoelastic behavior of flexible polyurethane/CNT nanocomposite foam, Eur. Polym. J. 90 (2017) 383–391, https://doi.org/10.1016/j.eurpolymj.2017.03.042.

[22] G. Sui, D. Liu, Y. Liu, W. Ji, Q. Zhang, Q. Fu, The dispersion of CNT in TPU matrix with different preparation methods: solution mixing vs melt mixing, Polymer 182 (2019), 121838, https://doi.org/10.1016/j.polymer.2019.121838.

[23] G. Barra, L. Guadagno, B. Simonet, B. Santos, The influence of different dispersion methods on the size of the aggregate of CNTs in epoxy resin for the manufacturing of carbon fiber reinforced composites, AIP Conf. Proc. 1736 (2016), 020158, https://doi.org/10.1063/1.4949733.

[24] M. Yourdkhani, W. Liu, S. Baril-Gosselin, F. Robitaille, P. Hubert, Carbon nanotube-reinforced carbon fibre-epoxy composites manufactured by resin film infusion, Compos. Sci. Technol. 166 (2018) 169–175, https://doi.org/10.1016/j.compscitech.2018.01.006.

[25] N. Sezer, M. Koç, Stabilization of the aqueous dispersion of carbon nanotubes using different approaches, Therm. Sci. Eng. Prog. 8 (2018) 411–417, https://doi.org/10.1016/j.tsep.2018.09.011.

[26] P. Mayuri, N. Saravanan, A.S. Kumar, A bioinspired copper 2,2-bipyridyl complex immobilized MWCNT modified electrode prepared by a new strategy for elegant electrocatalytic reduction and sensing of hydrogen peroxide, Electrochim. Acta 240 (2017) 522–533, https://doi.org/10.1016/j.electacta.2017.04.082.
[27] M.S. Ata, R. Poon, A.M. Syed, J. Milne, I. Zhitomirsky, New developments in non-covalent surface modification, dispersion and electrophoretic deposition of carbon nanotubes, Carbon 130 (2018) 584–598, https://doi.org/10.1016/j.carbon.2018.01.066.
[28] S. Gao, B.S. Villacorta, L. Ge, T.E. Rufford, Z. Zhu, Effect of sonication and hydrogen peroxide oxidation of carbon nanotube modifiers on the microstructure of pitch-derived activated carbon foam discs, Carbon 124 (2017) 142–151, https://doi.org/10.1016/j.carbon.2017.08.036.
[29] G. Singer, P. Siedlaczek, G. Sinn, H. Rennhofer, M. Mĭcušík, M. Omastová, M. M. Unterlass, J. Wendrinsky, V. Milotti, F. Fedi, T. Pichler, H.C. Lichtenegger, Acid free oxidation and simple dispersion method of MWCNT for high-performance CFRP, Nanomaterials (Basel) 8 (2018) 912–929, https://doi.org/10.3390/nano8110912.
[30] N. Dilsiz, J.P. Wightman, Effect of acid–base properties of desized and sized carbon fibers on fiber/epoxy matrix adhesion, Colloids Surf. A Physicochem. Eng. Asp. 164 (2000) 325–336, https://doi.org/10.1016/S0927-7757(99)00400-8.
[31] D.K. Owen, R.C. Wendt, Estimation of the surface free energy of polymer, J. App. Poly. Sci. 13 (1969) 1741–1747, https://doi.org/10.1002/app.1969.070130815.
[32] J.H. Kim, D.J. Kwon, P.S. Shin, Y.M. Baek, H.S. Park, K.L. DeVries, J.M. Park, New evaluation of interfacial properties and damage sensing in CFRC by VARTM using 3D ER mapping, Compos. B Eng. 155 (2018) 178–186, https://doi.org/10.1016/j.compositesb.2018.08.010.
[33] Y. Peng, H. Liu, Effects of oxidation by hydrogen peroxide on the structures of multiwalled carbon nanotubes, Ind. Eng. Chem. Res. 45 (2006) 6483–6488, https://doi.org/10.1021/ie0604627.
[34] V. Datsyuk, M. Kalyva, K. Papagelis, J. Parthenios, D. Tasis, A. Siokou, I. Kallitsis, C. Galiotis, Chemical oxidation of multiwalled carbon nanotubes, Carbon 46 (2008) 833–840, https://doi.org/10.1016/j.carbon.2008.02.012.
[35] R. Benlikaya, P. Slobodian, P. Riha, Enhanced strain-dependent electrical resistance of polyurethane composites with embedded oxidized multiwalled carbon nanotube networks, J. Nanomater. 2013 (2013), 327597, https://doi.org/10.1155/2013/327597.